# Transport properties of pancreatic cancer describe gemcitabine delivery and response

Eugene J. Koay,[1,2] Mark J. Truty,[3] Vittorio Cristini,[4] Ryan M. Thomas,[5,6] Rong Chen,[7] Deyali Chatterjee,[8] Ya'an Kang,[8] Priya R. Bhosale,[9] Eric P. Tamm,[9] Christopher H. Crane,[1] Milind Javle,[7] Matthew H. Katz,[8] Vijaya N. Gottumukkala,[10] Marc A. Rozner,[10] Haifa Shen,[2] Jeffery E. Lee,[8] Huamin Wang,[11] Yuling Chen,[7] William Plunkett,[7] James L. Abbruzzese,[12] Robert A. Wolff,[7] Gauri R. Varadhachary,[7] Mauro Ferrari,[2] and Jason B. Fleming[8]

[1]Division of Radiation Oncology, University of Texas M.D. Anderson Cancer Center, Houston, Texas, USA. [2]Department of Nanomedicine, Houston Methodist Research Institute, Houston, Texas, USA. [3]Department of Hepatobiliary and Pancreas Surgery, Mayo Clinic College of Medicine, Rochester, Minnesota, USA. [4]Department of Pathology, University of New Mexico, Albuquerque, New Mexico, USA. [5]Department of Surgery, University of Florida College of Medicine, Gainesville, Florida, USA. [6]Department of Surgery, North Florida/South Georgia VA Medical Center, Gainesville, Florida, USA. [7]Division of Cancer Medicine, [8]Division of Surgical Oncology, [9]Department of Diagnostic Radiology, [10]Department of Anesthesiology, and [11]Department of Pathology, University of Texas M.D. Anderson Cancer Center, Houston, Texas, USA. [12]Division of Medical Oncology, Duke Cancer Institute, Durham, North Carolina, USA.

***Background*. The therapeutic resistance of pancreatic ductal adenocarcinoma (PDAC) is partly ascribed to ineffective delivery of chemotherapy to cancer cells. We hypothesized that physical properties at vascular, extracellular, and cellular scales influence delivery of and response to gemcitabine-based therapy.**

***Methods*. We developed a method to measure mass transport properties during routine contrast-enhanced CT scans of individual human PDAC tumors. Additionally, we evaluated gemcitabine infusion during PDAC resection in 12 patients, measuring gemcitabine incorporation into tumor DNA and correlating its uptake with human equilibrative nucleoside transporter (hENT1) levels, stromal reaction, and CT-derived mass transport properties. We also studied associations between CT-derived transport properties and clinical outcomes in patients who received preoperative gemcitabine-based chemoradiotherapy for resectable PDAC.**

***Results*. Transport modeling of 176 CT scans illustrated striking differences in transport properties between normal pancreas and tumor, with a wide array of enhancement profiles. Reflecting the interpatient differences in contrast enhancement, resected tumors exhibited dramatic differences in gemcitabine DNA incorporation, despite similar intravascular pharmacokinetics. Gemcitabine incorporation into tumor DNA was inversely related to CT-derived transport parameters and PDAC stromal score, after accounting for hENT1 levels. Moreover, stromal score directly correlated with CT-derived parameters. Among 110 patients who received preoperative gemcitabine-based chemoradiotherapy, CT-derived parameters correlated with pathological response and survival.**

***Conclusion*. Gemcitabine incorporation into tumor DNA is highly variable and correlates with multiscale transport properties that can be derived from routine CT scans. Furthermore, pretherapy CT-derived properties correlate with clinically relevant endpoints.**

***Trial registration*. Clinicaltrials.gov NCT01276613.**

***Funding*. Lustgarten Foundation (989161), Department of Defense (W81XWH-09-1-0212), NIH (U54CA151668, KCA088084).**

## Introduction

Pancreatic ductal adenocarcinoma (PDAC) is one of the most lethal malignancies, and 2 decades of clinical research have demonstrated minimal improvement in the median overall survival of patients (1, 2). Although several biological explanations have been proposed for the poor therapeutic outcomes of patients, physical phenomena may also contribute to the significant difficulty in treating this disease (1). Preclinical and clinical investigations have suggested that the therapeutic resistance associated with PDAC (2) may be partly attributed to ineffective chemotherapy delivery to cancer cells (3, 4).

Solid tumors, such as PDAC, often have mass transport properties that differ from those of normal tissues (5–11). PDAC exhibits several pathological features that can be considered physical barriers to effective drug delivery, including disorganized, leaky, and nonfunctional vasculature (12–14); characteristically dense stroma (9); and deregulated cellular transport proteins (15). The leaky vasculature of solid tumors can create high interstitial fluid pressure (6), preventing the movement of chemotherapy from the vasculature to the extracellular compartment. The extracellular compartment of PDAC is usually a dense stromal (desmoplastic) reaction

**Authorship note:** Eugene J. Koay, Mark J. Truty, and Vittorio Cristini contributed equally to this work.

**Conflict of interest:** The authors have declared that no conflict of interest exists.

**Note regarding evaluation of this manuscript:** Manuscripts authored by scientists associated with Duke University, The University of North Carolina at Chapel Hill, Duke-NUS, and the Sanford-Burnham Medical Research Institute are handled not by members of the editorial board but rather by the science editors, who consult with selected external editors and reviewers.

**Citation for this article:** *J Clin Invest.* 2014;124(4):1525–1536. doi:10.1172/JCI73455.

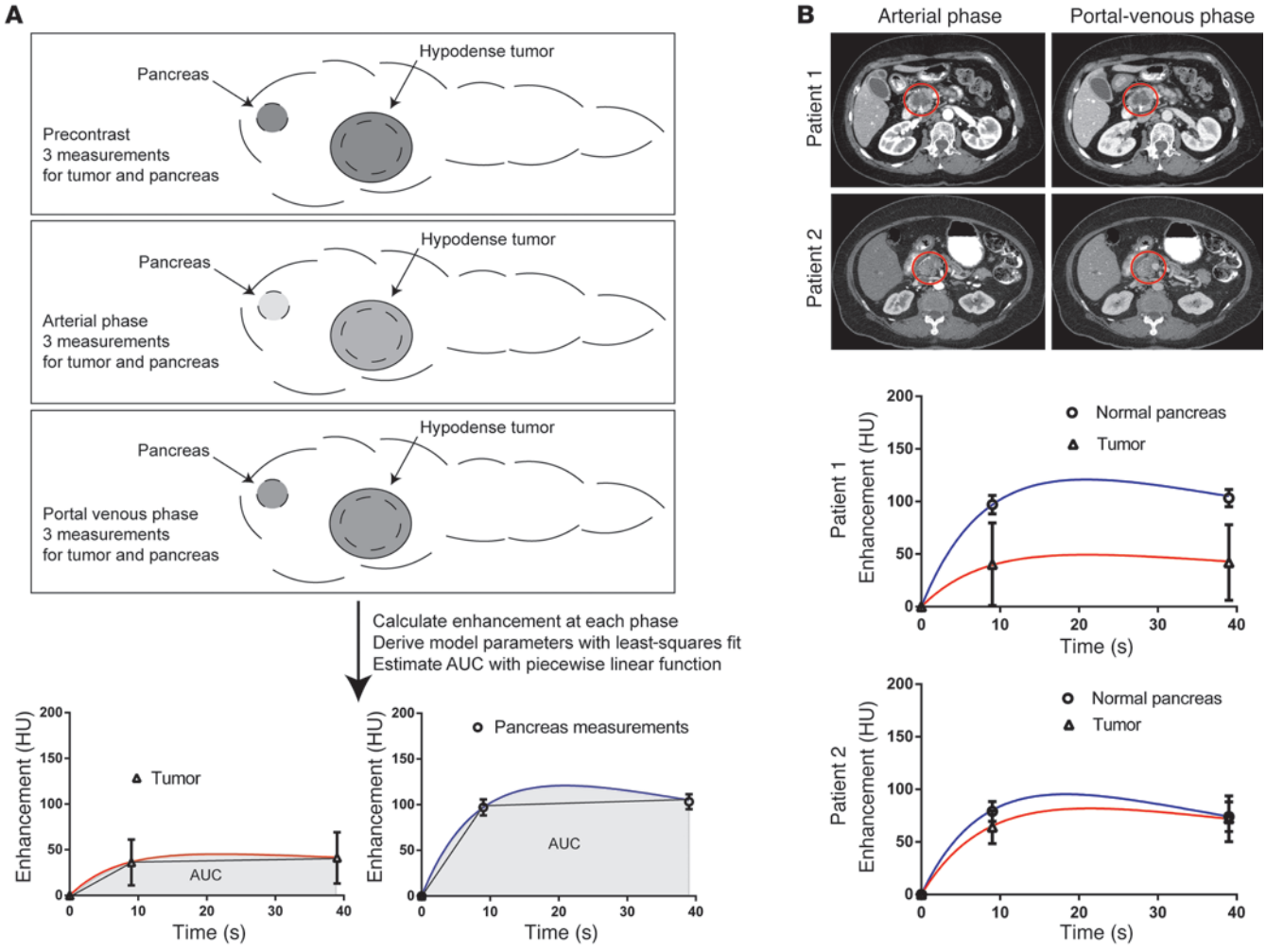
A
Pancreas
Hypodense tumor
Precontrast
3 measurements
for tumor and pancreas
Arterial phase
3 measurements
for tumor and pancreas
Portal venous phase
3 measurements
for tumor and pancreas
Calculate enhancement at each phase
Derive model parameters with least-squares fit
Estimate AUC with piecewise linear function
Enhancement (HU)
Tumor
AUC
Time (s)
Pancreas measurements
B
Arterial phase
Portal-venous phase
Patient 1
Patient 2
Normal pancreas
Tumor
C
Tissue
Pancreas
Tumor
P = 0.02
R² = 0.03
P < 0.0001
R²=0.37
AUC (HU•s)
Aorta enhancement (HU)
D
P < 0.0001
Distribution (%)

**Figure 1**
Deriving transport properties of pancreatic tumors from routine CT scans. (**A**) Measurement technique. The pancreatic protocol involved well-timed scans in relation to contrast injection: precontrast, arterial phase, and portal venous phase (dashed lines denote representative measurement area). Systematic measurements of the pancreatic tumor and normal pancreas were recorded, and a model was developed to derive transport properties from these measurements. The model function can be integrated with time to derive AUC, and a simple piecewise linear function can be used to estimate AUC. (**B**) Scans from 2 patients with different enhancement patterns in the normal pancreas and pancreatic tumor are shown. The density changed with time due to intravasation of contrast into the tissues. Modeled density changes are shown, demonstrating that the model provides transport parameters for each patient's normal tissue (blue line) and cancer (red line). (**C**) AUC representing the time integral of enhancement in the tissue of interest. The model was validated by comparing tissue-derived parameters with the enhancement in the aorta at the level of the celiac axis, which should reflect enhancement in the tissues. The graph for all 176 patients with pancreatic protocol CTs in this study shows how normal pancreas closely reflected aortic enhancement, whereas pancreatic tumors had higher variability. (**D**) Distributions of the parameter AUC from CT scans of 176 patients, grouped by pancreatic tissue type. Significant differences in the distribution of transport parameters were evident between normal pancreas and pancreatic tumor, with tumors exhibiting worsened transport properties.

that has been shown to influence the delivery of and response to gemcitabine in preclinical models (3, 9, 13). Indeed, differential mass transport is the basic principle that allows diagnostic radiologists to qualitatively differentiate between normal and pathological tissues in the pancreas. The pancreatic protocol CT scan is a diagnostic test that exemplifies this differential mass transport principle (16). PDACs are typically hypodense compared with the normal pancreas during the timed phases of the diagnostic test.

Altered mass transport can be seen at the cellular level as well. Human equilibrative nucleoside transporter (hENT1) represents the primary transport protein for gemcitabine and other nucleoside analogs to enter the cellular compartment and ultimately inhibit DNA replication. Studies have shown that hENT1 has variable expression in human PDAC that correlates with outcome after adjuvant gemcitabine therapy (15), presumably due to differential gemcitabine uptake at the cellular level based on high or low levels of functional hENT1 expression. Gemcitabine, like other drugs with intracellular targets, must traverse the vascular, extracellular, and cellular compartments of solid tumors like PDACs to ultimately have an effect. These different physical barriers span orders of magnitude (meters to angstroms), highlighting the significant challenge of drug delivery.

In this study, we hypothesized that multiscale transport phenomena (6–8) influence delivery of and response to gemcitabine-based therapy in human PDAC. We studied transport phenomena in human PDAC by using the pancreatic protocol CT scans of patients and conducting a first-in-kind clinical trial of intraoperative gemcitabine infusion during curative resection of PDAC. In the clinical trial, we quantified the transport properties of the vasculature, the extracellular matrix, and the cellular protein hENT1, assessing their correlations with gemcitabine DNA incorporation. We also investigated how the transport properties correspond with outcomes after neoadjuvant gemcitabine-based chemoradiation for resectable PDAC.

## Results

*Development and validation of a novel mass transport model for human pancreatic protocol CT scans*. We hypothesized that mathematical modeling of the changes in enhancement of the tissues — measured in Hounsefield units (HU) — at sequential time points during the pancreatic protocol (precontrast, arterial, and portal-venous phases) could quantify the mass transport properties of individual PDACs.

We used multiple, systematic measurements obtained during the pancreatic protocol CT in a novel mathematical model to yield phenomenological parameters of mass transport that describe qualities of the pancreatic tissue (normal and tumor) and its surrounding vasculature (see Methods and Figure 1A).

The transport model consists of 1 ordinary differential equation describing the variable density $Y(t)$ (in HU) in the tissue as a function of time $t$ resulting from transfer of contrast agent molecules through the vessel walls at rate $R$ (in $s^{-1}$) and clearance rate from the vasculature $R_c$ (in $s^{-1}$):

$$dY/dt = R \times [Y^V_{max} \times \exp(-R_c \times t) - Y] \quad \text{(Equation 1)}$$

where $Y^V_{max}$ represents the (imposed) level of density within the microvasculature. Equation 1 is solved for initial condition $Y(0) = 0$, giving the solution for $Y(t)$ (see Figure 1):

$$Y(t) = Y^V_{max} \times R \times [\exp(-R_c \times t) - \exp(-R \times t)]/[R - R_c] \quad \text{(Equation 2)}$$

2 other model parameters can be derived from the intrinsic variables of the model ($R$, $R_c$, and $Y^V_{max}$; see Methods): maximum enhancement of tissue ($Y^T_{max}$) and initial influx rate of contrast ($R_0$). The model function can also be integrated over time to give an area under the model-predicted enhancement curve (AUC).

Using these methods, we analyzed pretherapy pancreatic protocol CTs from 176 patients with localized primary PDAC. 3 patient cohorts were studied: 12 who received i.v. infusion of gemcitabine during tumor resection on clinical trial (11 of which had evaluable CT scans; Supplemental Table 1; supplemental material available online with this article; doi:10.1172/JCI73455DS1), 110 who received gemcitabine-based chemoradiotherapy for potentially resectable PDAC (Supplemental Table 2), and 55 who received upfront tumor resection (Supplemental Table 3). The group of 55 patients served as the learning dataset in model development (Methods and Supplemental Table 4), providing a range of constraints for the parameters $R$ and $R_c$ for analysis of the other patient sets.

Image analysis identified a broad range of enhancement patterns for the patients (Figure 1B), which indicates that the pancreatic protocol CT can be used not only for diagnostic purposes, but also for derivation of the physical properties of each patient's unique tumor. For normal pancreas tissue, AUC significantly correlated with arterial phase enhancement in the aorta at the level of the celiac artery for each patient (Figure 1C). Thus, the measurements and modeling of the behavior of the normal pancreatic tissue accounted for any differences in contrast dose and patient physiology (e.g., cardiac output). Similar analysis of the tumor tissues showed greater variability than those found in normal pancreas (Figure 1C and Supplemental Table 5). The transport properties of pancreatic tumors and normal pancreas were significantly different (Figure 1D), showing that the tissues can be quantitatively differentiated.

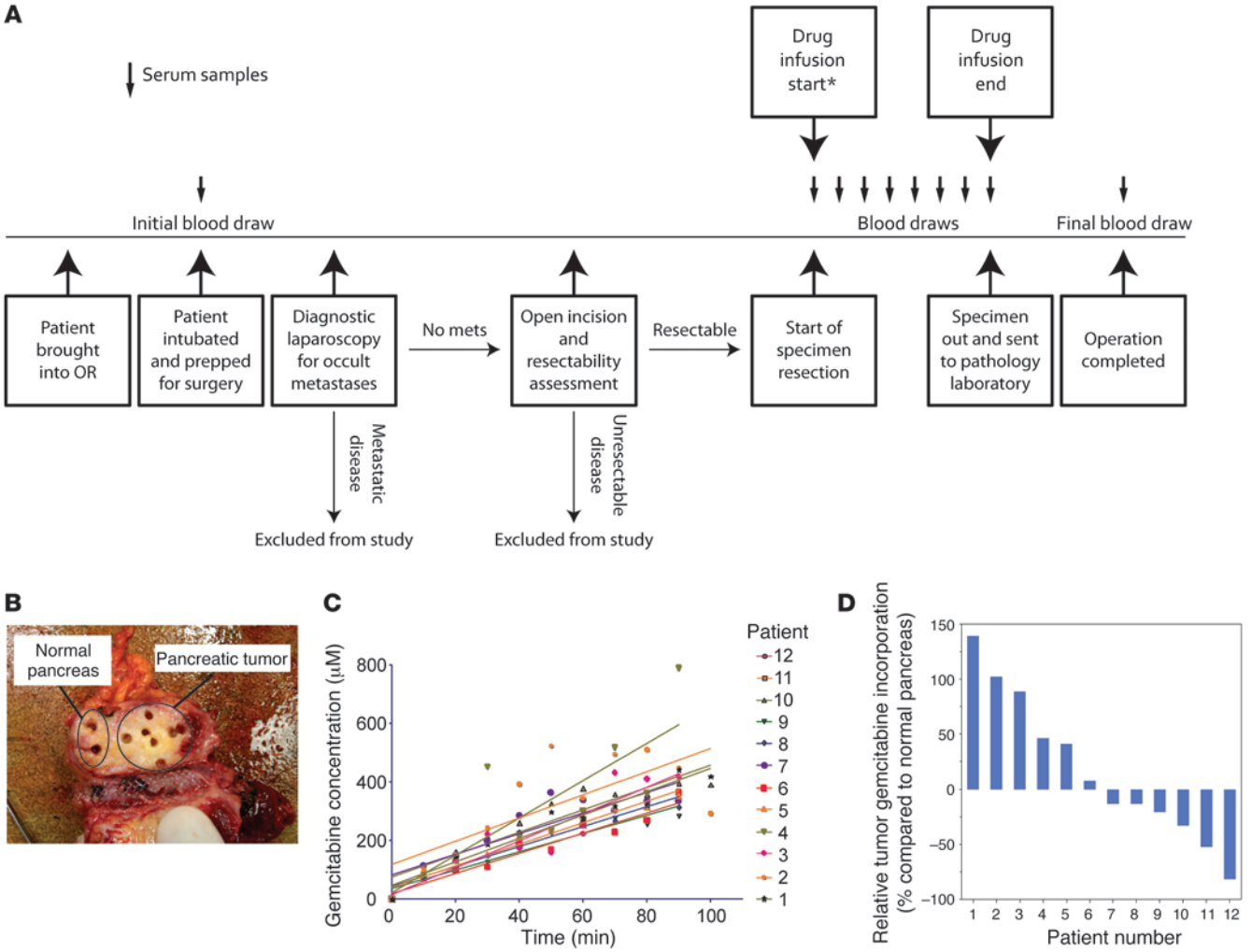


**Figure 2**

Clinical trial of intraoperative gemcitabine. (**A**) Trial design. Patients were evaluated for appropriateness for resection before infusion of gemcitabine. Gemcitabine infusion was initiated at the start of resection (asterisk; 50–100 minutes prior to specimen removal, with time dependent on drug dose) and infused at a fixed rate (see Methods). Pathological analysis and quantitative assessment of gemcitabine incorporation were then performed. (**B**) Immediately after tumor resection, specimens were collected using standard surgical pathology techniques, and punch biopsies of the tumor and normal pancreas were taken to measure gemcitabine incorporation into DNA. (**C**) Blood samples were collected at regular intervals during the intraoperative infusion of gemcitabine, so that drug concentration could be measured by HPLC and intravascular pharmacokinetics could be analyzed. The similar slopes of the lines and the tight distribution of serum gemcitabine concentrations at each time point indicate that the infusion conditions were similar for all 12 trial patients. (**D**) DNA was extracted from tumor biopsy samples and analyzed for gemcitabine incorporation (measured relative to deoxyguanosine) into the DNA of pancreatic tumor cells. A positive value indicates more gemcitabine incorporation into the tumor compared with normal pancreas; a negative value indicates less. Marked variability was observed in the amount of gemcitabine incorporated for the 12 trial patients.

To assess the appropriateness of the developed model, we compared the model-derived AUC with an estimate of AUC using a simple piecewise linear function (see Methods). There was a 1:1 linear relationship between the estimated and model-derived AUC parameters (Supplemental Figure 1), which was expected since our model is continuous; moreover, the simple piecewise linear approximation can be easily translated to clinical practice, as only a straightforward calculation is necessary.

*Multiscale transport factors influence delivery of gemcitabine to human PDAC cells.* We conducted a first-in-kind, prospective clinical trial in which gemcitabine was intravenously infused during curative resection of 12 patients with localized primary PDAC (Supplemental Table 1 and Figure 2A). Our objective was to understand whether transport-related factors influence gemcitabine incorporation into cellular DNA. We developed and optimized methods to quantitatively measure gemcitabine incorporation into DNA of cells in the tumor, blood samples, and other tissue (Figure 2B and Supplemental Figures 2–4). Gemcitabine pharmacokinetics and hematological toxicity were similar for all patients (Figure 2C and Supplemental Figure 5). Despite similar intravascular pharmacokinetics and well-controlled infusion conditions, levels of gemcitabine incorporation into DNA of cells in the tumors and normal pancreas were highly variable among patients (Figure 2D). Notably, gemcitabine incorporation in the tumors ranged from sub- to supranormal pancreas levels.

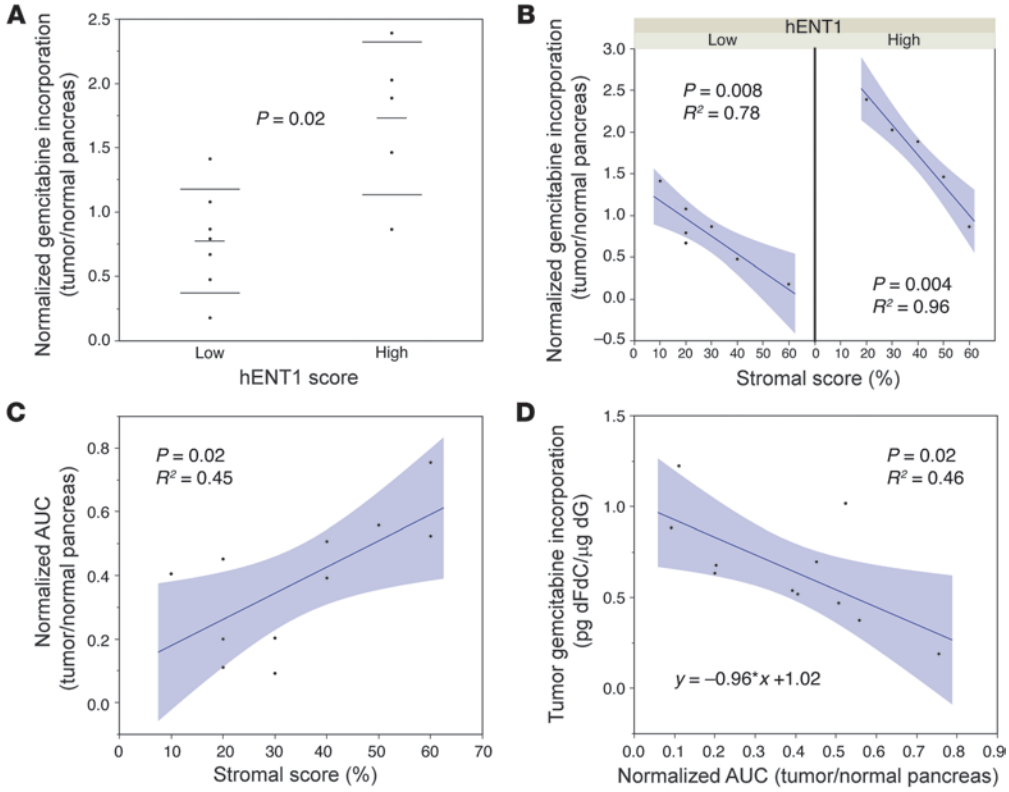


**Figure 3**
Correlations between transport properties and gemcitabine incorporation. (**A**) Normalized gemcitabine incorporation for each patient on the clinical trial of intraoperative gemcitabine infusion during PDAC resection, measured using specimens obtained directly from the tumor (see Figure 2B). Surgical specimens were scored for hENT1 staining (see Supplemental Table 6). A significant difference was observed in the normalized gemcitabine incorporation when divided by hENT1 score (2-tailed *t* test; mean and SD indicated by short and long lines, respectively). (**B**) Stroma amount was scored independently by a pathologist, and gemcitabine incorporation in the tumor and normal pancreas were measured. After accounting for hENT1 score, a significant inverse correlation was seen with normalized gemcitabine incorporation (linear regression). (**C**) Pretherapy CTs of each patient in the clinical trial of intraoperative gemcitabine infusion during PDAC resection were derived, and the normalized CT-derived parameter AUC was plotted against the stromal scores from surgical pathology for the corresponding patient. A direct linear correlation was observed. (**D**) Normalized AUC was plotted against the measured gemcitabine (dFdC) incorporation into pancreatic tumor cell DNA (expressed relative to deoxyguanosine [dG]). A significant inverse correlation was observed (linear regression), in agreement with the inverse correlation found for the stromal score (**B**), which directly correlated with the normalized CT parameter AUC (**C**). The equation indicates how the CT parameter may be used to predict gemcitabine incorporation in future clinical trials.

We hypothesized that the variability of gemcitabine incorporation in tumors among the patients could be explained by mass transport phenomena. We discovered that in all correlations of transport phenomena, normalization of 1 variable in the correlation was important (e.g., normalized dependent variable vs. non-normalized independent variable, or vice versa). Using appropriate measurements in normal pancreas as the normalization factor reduced variability in the correlations (Supplemental Figure 6). Variability may stem from biological differences among patients and minor differences in the acquisition timing of the CT scan.

Because extensive desmoplasia is a common feature of PDAC that reflects a putative stromal barrier to gemcitabine delivery and also impairs vasculature function (3, 9, 13, 14), we hypothesized that the stromal amount in the specimens would influence gemcitabine delivery. Upon initial evaluation, stromal score by itself did not correlate with tumor gemcitabine incorporation (Supplemental Figure 7). Considering that expression of the nucleoside transporter of gemcitabine, hENT1, correlates with outcome after adjuvant gemcitabine therapy in patients with PDAC (15) and our initial multiscale mass transport hypothesis (8), we hypothesized that hENT1 scoring would improve our correlations between stromal score and normalized gemcitabine incorporation. We first ranked patients by hENT1 staining intensity (Supplemental Table 6) and then assigned designations of high and low down the ranked order. We subsequently assessed correlations between stromal score and normalized gemcitabine incorporation for the high hENT1 and low hENT1 groups. Ultimately, we identified 5 patients with high hENT1 staining and 7 patients with low hENT1 staining (Supplemental Figure 8). Although the semiquantitative nature of hENT1 intensity scoring limits this methodology, the final classification was similar to previous work (15, 17). In this manner, we found that hENT1 score significantly correlated with normalized gemcitabine incorporation (Figure 3A). Consistent with our multiscale mass transport hypothesis, stromal score inversely correlated with normalized gemcitabine incorporation after accounting for the hENT1 score (Figure 3B), as we had initially anticipated.

**Table 1**
Final multivariate overall survival model for 110 patients receiving gemcitabine-based chemoradiation for potentially resectable pancreatic cancer

| | Univariate model | | Multivariate model | |
|---|---|---|---|---|
| **Characteristic** | **Hazard ratio (95% CI)** | ***P*** | **Hazard ratio (95% CI)** | ***P*** |
| Normalized AUC[A] | 0.28 (0.11–0.69) | 0.006 | 0.20 (0.05–0.74) | 0.02 |
| Curative-intent resection[B] | 0.12 (0.07–0.22) | <0.0001 | 0.12 (0.07–0.23) | <0.0001 |

[A]*n* = 110. [B]*n* = 80 (yes); 30 (no). See Supplemental Table 7 for full univariate analyses.

Furthermore, we hypothesized that the CT-derived parameters would reflect tumor pathology and correlate with gemcitabine incorporation. We derived mass transport parameters for the 11 of 12 total clinical trial patients who had pretherapy pancreatic protocol CTs, and noted significant correlations between the CT-derived parameters and tumor stromal score within the surgical specimen (Figure 3C). Moreover, the normalized CT-derived parameters also inversely correlated with tumor gemcitabine incorporation (Figure 3D). Cellular proliferation was considered another possible determinant of gemcitabine incorporation, but we did not find a significant correlation with Ki67 score (Supplemental Figure 7).

*CT-derived transport parameters correlate with response to and survival after gemcitabine-based therapy*. Since the clinical trial suggested that physical mass transport properties could describe the variability in delivery of gemcitabine to the tumor cell DNA, we hypothesized that the transport properties could also describe the variable response to and outcome after gemcitabine-based therapies. To test this idea, we correlated the CT parameters with pathological response and survival of patients with PDAC after preoperative chemoradiation (18). We identified 110 patients who received gemcitabine-based chemoradiation and had evaluable pretherapy CT scans from 2 prospective clinical trials at our institution for potentially resectable PDAC (19, 20). From these 2 trials, a total of 66 patients — specifically, 55 (19) and 11 (20) — did not have evaluable CT scans, because the initial scan was either from another institution or not a pancreatic protocol CT. Of the 110 patients evaluated, 80 underwent a curative resection; the other 30 were unresectable after chemoradiation. Surgical resection and CT-derived parameter normalized AUC were the only variables that significantly correlated with overall survival in the entire cohort of 110 patients on both univariate and multivariate analyses (Table 1 and Supplemental Table 7). A subgroup analysis of the 80 patients who underwent resection revealed that patients with pathologically involved nodes after chemoradiation had poorer grades of response (proportion of viable cells, 0.31 ± 0.20) compared with patients with no pathologically involved nodes after neoadjuvant therapy (0.20 ± 0.16; $P = 0.02$); no other clinical or treatment-related factors correlated with pathological response or survival, except nor-

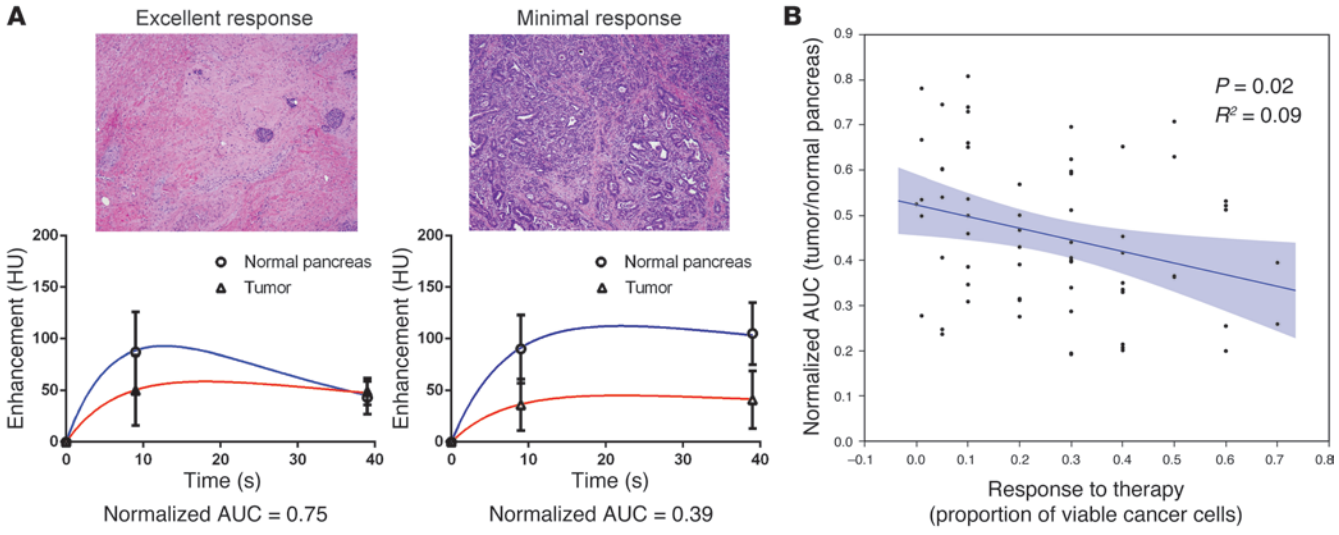


**Figure 4**
Correlations between transport properties and response. (**A**) Representative histology, CT profiles, and normalized AUC values for patients with excellent (trace viable tumor cells) and minimal (approximately 70% viable tumor cells) responses to therapy. The patient with an excellent response had higher normalized AUC than the patient with a minimal response. (**B**) Normalized AUC was measured from the pretherapy CT scans of the patients who underwent surgery for potentially resectable PDAC in 2 phase 2 clinical trials of preoperative gemcitabine-based regimens (19, 20). The pathological response to therapy was scored by a pathologist. Higher normalized AUC appeared to correlate with better pathological response (linear regression). Notably, Spearman rank-order correlation was also significant (–0.30; 95% CI, –0.51 to –0.05; $P = 0.02$).

**Table 2**
Final multivariate overall survival model for 80 patients with PDAC who underwent resection after gemcitabine-based chemoradiation

| | Univariate model | | Multivariate model | | Multivariate model | |
|---|---|---|---|---|---|---|
| **Characteristic** | **Hazard ratio (95% CI)** | ***P*** | **Hazard ratio (95% CI)** | ***P*** | **Hazard ratio (95% CI)** | ***P*** |
| Normalized AUC[A] | 0.26 (0.09–0.80) | 0.02 | — | — | 0.29 (0.04–0.86) | 0.03 |
| Surgical margin[B] | 1.44 (0.44–3.53) | 0.50 | 2.39 (0.56–7.06) | 0.21 | 1.36 (0.41–3.32) | 0.57 |
| Pathological stage[C] | 1.33 (0.81–2.22) | 0.25 | 1.23 (0.66–2.36) | 0.51 | 1.22 (0.73–2.04) | 0.45 |
| Pathological response[D] | 5.68 (2.08–15.35) | 0.0008 | 5.04 (1.72–14.93) | 0.003 | — | — |

[A]$n$ = 80. [B]$n$ = 4 (positive); 76 (negative). [C]$n$ = 44 (N1); 36 (N0). [D]$n$ = 65.

malized AUC (Supplemental Table 8). We observed distinct CT signatures in patients who had complete pathological responses compared with those with poor responses to therapy (Figure 4A), and the normalized CT-derived parameter AUC directly correlated with pathological response (Spearman rank-order correlation, –0.30; 95% CI, –0.51 to –0.05; $P$ = 0.02; Figure 4B). As previously observed by our group (18, 21), patients with better grades of pathological responses (i.e., fewer viable cells after therapy) had improved prognosis, and as response correlated directly with normalized AUC, patients with higher normalized AUC values also had improved prognosis (Supplemental Table 8). Multivariate analysis of the 80 patients who underwent resection confirmed that normalized AUC was an independent predictor of overall survival (Table 2).

An exploratory partitioning analysis identified a cutoff of 0.6 for normalized AUC. Applying this cutoff to the entire cohort of 110 patients showed that patients with high normalized AUC had significantly better outcome than those with low normalized AUC (40% vs. 15% survival rate at 5 years), independent of whether the patients had curative-intent surgery (Figure 5A and Supplemental Table 9). Additionally, the same cutoff for normalized AUC remained a significant predictor of survival in the 80 patients who underwent surgery, independent of margin status and lymph node involvement (Figure 5B and Supplemental Table 10).

## Discussion

While other cancers have seen significant improvements in overall survival during the past several decades, PDAC has continued to carry a dismal prognosis (2, 22). Advances in the understanding of PDAC genetics and biology have led to novel therapeutic strategies (3, 23, 24), but their application in PDAC has not yet improved clinical outcomes for patients (25–27). One of the challenges that may influence these outcomes is the delivery of the drug to its molecular target (8, 28), but the concept of mass transport characterization in human cancer has not been integrated into clinical practice. Here, we developed, validated, and applied methods to quantify mass transport for individual human PDAC tumors. Our results support the concept that these transport phenomena influence the delivery of and response to gemcitabine-based therapies (Figures 4–6). With further validation and optimization, our CT analysis method may find wide clinical application for both diagnostic and therapeutic-planning purposes, as the principles of mass transport can be applied to any human pathological process as well as a variety of therapeutic agents. The clinical trial design of intraoperative drug infusion is a critical component of our study of mass transport in PDAC, represents a novel platform by which to study mechanisms of targeted drug delivery, and complements our CT analysis. Combined, the methodologies we

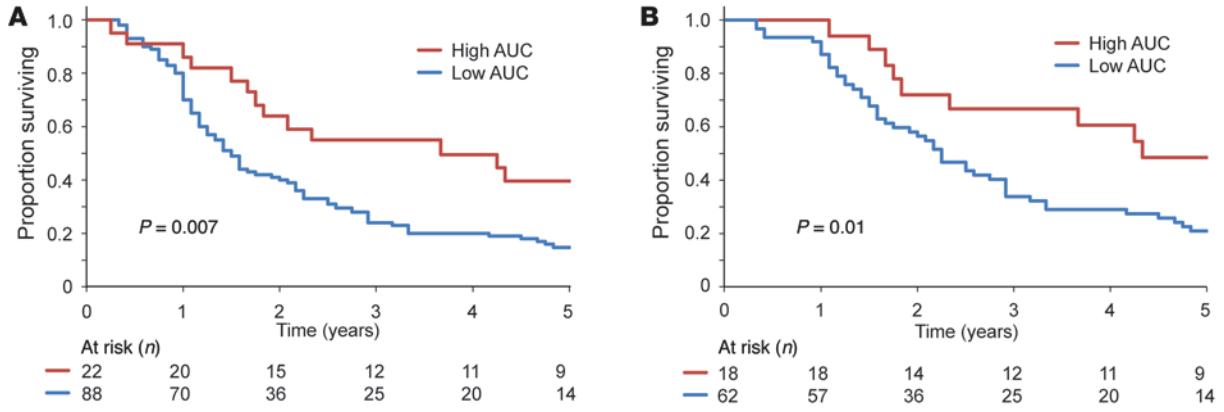


**Figure 5**
Correlations between transport properties and survival. (**A**) Using a partitioning analysis for all 110 patients who received gemcitabine-based therapy in 2 published phase II trials for potentially resectable PDAC (19, 20), a cutoff of 0.6 was identified for normalized AUC (values greater than 0.6 were considered high; all others were low). This designation separated patients with a good prognosis from those with a poor prognosis on univariate and multivariate analyses (see Supplemental Table 9). (**B**) Of the initial 110 patients who received gemcitabine-based therapies for potentially resectable PDAC, 80 underwent curative-intent surgery. When the same cutoff of 0.6 for normalized AUC was applied to these 80 patients, patients with good prognosis were again separated from those with poor prognosis. This finding was significant on univariate and multivariate analyses (see Supplemental Table 10).

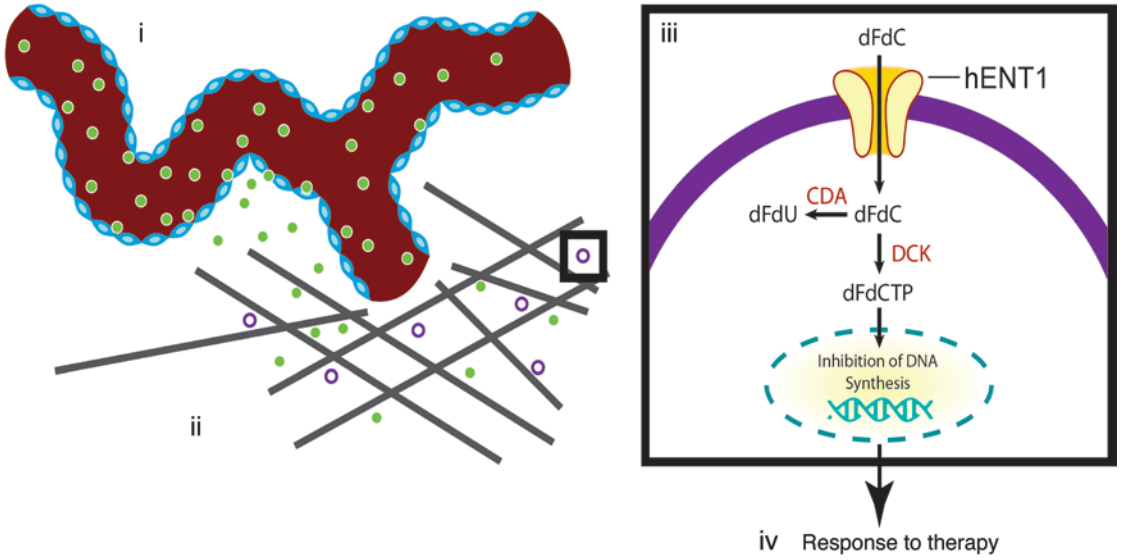


**Figure 6**
Multiscale transport model of response to therapy. (i) The CT-derived parameters describe vascular tissue transport qualities (Figure 1) and also reflect underlying histopathology (Figure 3). (ii) The clinical trial demonstrated highly variable drug delivery (Figure 2) and showed that more stroma led to less gemcitabine incorporation (Figure 3). (iii) The clinical trial also illustrated how hENT1 expression can influence gemcitabine incorporation (Figure 3). (iv) The response to and outcome after therapy correlated with the CT-derived parameters (Figures 4 and 5 and Tables 1 and 2). CDA, cytidine deaminase; DCK, deoxycytidine kinase; dFdU, 2′,2′ difluorodeoxyuridine; dFdCTP, 2′,2′ difluorodeoxycytidine triphosphate.

developed here and the results we obtained may lead to rational interventions for pancreatic cancer and other solid tumors that improve drug delivery and thereby extend survival for patients.

Our CT analysis can be integrated into existing standard-of-care diagnostic tests, such as the pancreatic protocol CT that is ubiquitously used clinically. Others have used dynamic contrast-enhanced (DCE) MRI (29, 30) and perfusion CT (31) to derive mass transport properties from imaging, correlating these properties with response to cancer therapy. In contrast to our mass transport analysis of the pancreatic protocol CT, DCE MRI and perfusion CT require another imaging test after the routine scan is performed, requiring increased contrast exposure for the patient and additional cost. The CT transport analysis we developed here can be integrated into the existing pancreatic protocol CT, enhancing it for applications beyond its current capabilities.

For instance, the parameters derived from our mass transport model describe qualities of the tissue of interest and its surrounding vasculature, and these quantitatively differentiated malignant from normal tissue processes by at least 2-fold (Figure 1D). This provides a stark contrast between tissues and offers evidence that mass transport is diminished or limited in pancreatic tumors compared with normal pancreas tissue, as has been postulated previously (5, 6, 8, 28). With further development, these quantitative differences in mass transport may help radiologists more clearly distinguish between normal and pathological processes. Therapeutic-planning applications can also be envisioned in which the pretreatment biophysical characterization of a patient's tumor is used to inform management decisions.

Toward this goal, our results showed how the CT-derived parameter normalized AUC correlated with gemcitabine incorporation (Figure 3D), pathological response (Figure 4B), and survival after gemcitabine-based therapies (Figure 5). It is notable that other model parameters had correlations (Supplemental Figure 6), but we focused on AUC because it is currently the most robust parameter. Specifically, by its definition as an integral over time, AUC is less sensitive to minor variations in CT acquisition and patient physiology compared with other model parameters. Our finding that the model parameter AUC could be approximated in a simple and accurate manner (Methods and Supplemental Figure 1) means that the technique can be performed at any institution without any complex algorithms or software, as long as the HU of the pancreatic tissues can be measured and the timing is known for each sequence of the pancreatic protocol CT scan, which is currently readily available. It is important to note, however, that the approximation of AUC would not have been possible without first identifying the appropriate analysis technique that the mathematical model defined and required (see Methods). Furthermore, the transport model provided scientific insight into the meaning of the imaging-derived parameters, such as AUC, as properties of mass transport. Better understanding of the observed phenomena is needed in order to integrate these concepts into the clinic.

Notably, we found that AUC could be used as a quantitative surrogate for stromal score (Figure 3C). This suggested that the CT parameters had a histopathological basis. Interestingly, both CT parameters and stromal score (after accounting for hENT1) were inversely correlated with gemcitabine DNA incorporation into the tumor (Figure 3, B and D). On the other hand, in the context of neoadjuvant chemoradiation for potentially resectable PDAC, we found that patients with tumors with higher normalized AUC had better responses and outcomes (Figure 4B, Figure 5, Table 2, and Supplemental Tables 9 and 10). One explanation may be that tumors with higher stromal scores have more abnormal vasculature; hence, these tumors with more stromal reaction

may exhibit arterial-venous shunting (12). This could manifest as higher values of transport parameters such as AUC, but lower levels of chemotherapy delivery because of mismatch between convective and diffusion-based transport of gemcitabine, preventing the cells from exposure to drug. Despite wide variability, it is notable that there was measurable drug delivery in all patients in our clinical trial of intraoperative gemcitabine infusion. It is possible that any drug delivery may be enough to sensitize cells to radiation, and radiation is likely the main determinant of response in the context of neoadjuvant chemoradiation. Moreover, it is possible that greater enhancement may correlate with better oxygenation, an important factor in radiation sensitivity. Future efforts will investigate how physical properties influence the response of tumors to cytotoxic therapies.

Although the association between the vascular and extracellular properties of the tissue needs further clarification, the data from our clinical trial of intraoperative drug infusion in 12 patients support our multiscale transport hypothesis (Figure 6). First, we observed a correlation between CT-derived vascular properties and gemcitabine incorporation. Second, our data provided evidence that the stroma impairs drug delivery by acting as a physical barrier to chemotherapy delivery or by disrupting vascular function (3, 9, 13, 14), as tumors with higher stromal scores had lower gemcitabine DNA incorporation (Figure 3B). This is in line with expectations based on studies using animal models of PDAC (3, 9, 13, 14), but no prior human data have shown an association between stromal amount and actual quantified drug delivery, as demonstrated here. Interestingly, we had to account for transport at the molecular scale (i.e., hENT1 expression) to show a significant correlation between tumor gemcitabine incorporation and stromal score.

In fact, there was overlap in tumor gemcitabine incorporation between patients with low and high hENT1 scores (Figure 3, A and B). Notably, one of the seminal studies of hENT1 in PDAC demonstrated an association between hENT1 expression and outcome, but not delivery (15). This study was in the context of adjuvant gemcitabine, meaning that the primary tumor and its stroma had been removed. Thus, the benefit of the chemotherapy was an effect on microscopic cancer cells. The sequential influence of the primary tumor's multiscale transport processes on the delivery of chemotherapy to cells (Figure 6) would not apply in the adjuvant setting. Interestingly, hENT1 level by itself does not seem to correlate with prognosis in the neoadjuvant setting (32), also supporting our multiscale transport hypothesis. Thus, our data are consistent with previous preclinical work and clinical observations, but they are unique in that they are the first demonstration that drug delivery in PDAC may depend on multiscale transport phenomena. In light of previous clinical studies of hENT1, our results emphasize that a single molecular biomarker (i.e., low or high hENT1) is likely not sufficient to select and enrich for those patients who would benefit from novel gemcitabine formulations in the primary disease setting. Furthermore, our data strongly support the Transport Oncophysics concept of multiscale mass transport deregulation (e.g., vascular, extracellular, and cellular) as a hallmark of cancer (8) and illustrate how these transport phenomena may be used to individualize clinical cancer management. Ongoing efforts will validate our initial findings in a second cohort of patients and test whether pretherapy CT imaging analysis can predict gemcitabine incorporation.

Toward the goal of individualization, our unique clinical trial platform can be used to study biological, pathological, and physical correlates of drug delivery in humans. Others have evaluated drug delivery in humans during therapy (33) or measured transport-related changes after chemotherapy (34), but no trial to our knowledge has analyzed the mass transport characteristics of the tumor that may have influenced drug delivery. In the development of this clinical trial, we performed extensive calibration, validation, and correlative studies (Supplemental Figures 2–4, 7, and 8). We also demonstrated that this trial design and methodology were safe (Supplemental Figure 5). By understanding the factors that influence drug delivery in humans with PDAC, we hope to develop rational interventions that improve therapeutic outcomes. In particular, one can envision using the intraoperative drug infusion clinical trial platform to test methods to alter the physical environment of the tumor, thereby increasing drug delivery, which provides a rationale for future clinical trials that aim to improve outcomes with these strategies.

Along these lines, our data indicate that some tumors may have physical properties that respond well to chemoradiation. Our finding that normalized AUC correlated with overall survival was expected, because it expanded on our previously published work of a physical mechanism describing how measurable diffusion-based properties of tumors from histopathology and contrast-enhanced CTs correlate with response to chemotherapy (11). It is conceivable that these physical properties are related to underlying biological processes. By investigating how the underlying molecular biology of the tumor and host may affect these biophysical signatures, targeted therapies, including emerging companion diagnostics (35), that modify the biophysical environment (stroma) of the tumor could be used to alter and track the properties of tumors for improved delivery and efficacy of systemic agents, shifting the biophysical profile along the observed response relationship (Figure 4B). This targeting of physical resistance could complement targeting of biological resistance; in some instances, these may be one and the same.

Considering their robust correlations with gemcitabine incorporation, pathological response, and oncologic outcome, CT-derived mass transport parameters represent biophysical markers that may have potentially significant implications for cancer medicine. Further development of diagnostic tests that simultaneously allow radiologic cancer staging as well as biophysical tumor profiling is warranted. The concept of individually tailored cancer therapy based on biophysical characterization is also supported by our present findings, as patients with good response to therapy appeared to have different physical properties compared with those with poorer responses. Our clinical trial platform of intraoperative drug infusion during resection suggests that the sequential contributions of vascular, extracellular, and cellular transport influence gemcitabine incorporation. Future investigations using this trial platform will aim to better understand these transport mechanisms, validate our findings, and develop rational therapeutic interventions for patients. In summary, the present work introduces and strongly supports the notion of quantitative biophysical markers that may provide clinically useful data to help direct cancer treatment and thereby improve the survival of patients with PDAC and, conceivably, other solid tumors.

## Methods

### *CT mass transport model*

*Model assumptions*. For the model, microvasculature enhancement ($Y^V(t)$) is described by a first-order decaying exponential at a rate $R_c$:

$$Y^V(t) = Y^V_{max} \times \exp(-R_c \times t) \quad \text{(Equation 3)}$$

$t = 0$ is defined as the time when $Y^V(t)$ is maximum (i.e., $Y^V(0) = Y^V_{max}$). At M.D. Anderson, bolus tracking of the aorta has been used since 2006, whereby a value of 100 HU in the aorta triggers the countdown to start the arterial phase scan (16 seconds later for a 16 detector scanner and 20 seconds later for a 64 detector scanner). This bolus tracking method improves the chances of observing differences in contrast uptake in pancreatic tissues by reducing differences in cardiac output for patients (36). We assumed that the model $t = 0$ occurred halfway between the bolus trigger of 100 HU and the beginning of the arterial phase, which would allow the contrast bolus to go through the cardiac circulation and reach the supplying vasculature of the pancreatic tissues. This assumption for the model $t = 0$ is well supported by previous work (37). For patients who had pancreatic protocol CTs prior to 2006, the timing in relation to the start of contrast infusion was the same as those who received scans after 2006. We performed sensitivity analyses to determine the effect of slight variations in the timing of the tests on the observed correlations (see Supplemental Figure 6). The model also assumes that the contribution of recirculation of contrast to the enhancement of the tissues is negligible during the test, as the arterial and portal venous phases are completed in just over 1 minute after the start of contrast infusion.

*Derivation of model parameters*. Model parameters were estimated for each patient by performing least-square fits of the solution of the model for the variable density (Equation 2) to the 3-timepoint CT measurements (in HU) at $t = 0$ ($Y(0) = 0$ for all patients because precontrast density was subtracted), $t_{arterial}$ (8 seconds for 16 detector scanner and 10 seconds for 64 detector scanner, using arterial phase density measurement minus precontrast phase density measurement in same tissue region of patient), $t_{venous}$ (38 seconds for 16 detector scanner and 40 seconds for 64 detector scanner, using portal venous phase measurement minus precontrast phase density measurement in same tissue region of patient) (for example, see Figure 1). The model definitions for $t_{arterial}$ and $t_{venous}$ corresponded to 40 and 70 seconds, respectively, after the start of contrast infusion, which are traditionally in the range of ideal times for acquisition (36).

Additionally, 2 important variables can be derived from the model (note that neither can actually be measured). The first is the initial slope or initial time derivative, $R_0$, of the predicted tissue density profile:

$$\text{At } t = 0,\ dY/dt = R_0 = Y^V_{max} \times R \quad \text{(Equation 4)}$$

The second is the predicted maximum value of density attained within tissue ($Y^T_{max}$), which may happen outside of the time window of the CT measurements:

$$\text{At } t = \log(R/R_c)/(R - R_c),\ dY/dt = 0, \text{ and } Y^T_{max} = Y^V_{max} \times (R/R_c)^{-Rc/(R-Rc)} \quad \text{(Equation 5)}$$

Note that, as expected, for all $t$, $Y(t) \le Y^T_{max} < Y^V_{max}$, as the value of density in the tissue cannot exceed the initial amount delivered to the microvasculature from the aorta.

The parameter AUC represents the time integral of the model-predicted enhancement function (Equation 2) from $t = 0$ to $t_{venous}$. We tested the appropriateness of the model by approximating AUC using a simple linear piecewise function. Essentially, we estimated AUC as the sum of the area of a triangle and a trapezoid (Figure 1A). In addition to showing the appropriateness of the model, this estimate of AUC is important for the clinical translation of our CT analysis, as the calculation is straightforward and can be done at any institution without additional algorithms or software.

### *CT measurements*

All analyses were performed on patients who were part of M.D. Anderson IRB-approved protocols. Enhancement (defined as postcontrast minus precontrast density) of pancreatic tumors showed considerable heterogeneity. For this study, we used multiple systematic measurements of the visualized tumors. 3 HU measurements from the hypodense region of the tumor were made. The same regions were sampled at each phase of the pancreatic protocol CT. Similarly, 3 measurements from the normal pancreas that was not obstructed by the tumor were made during each phase of the CT. The averages for the tumor and normal pancreas were used to derive mass transport properties using Equation 2.

### *Clinical trial of intraoperative gemcitabine infusion*

*Patients*. 12 patients with PDAC were enrolled on an IRB-approved protocol (Clinicaltrials.gov NCT01276613; Table 1). Written informed consent was obtained from all patients. All patients had cytologic or histologic proof of adenocarcinoma of the pancreas prior to treatment. Patients were staged with a physical exam, chest radiography, and contrast-enhanced CT, and only potentially resectable patients were eligible, as determined by the operative surgeon per previous criteria (38). There was no upper age restriction, and patients with Karnofsky performance status greater than 70 were eligible. All patients required adequate renal, hepatic, and bone marrow function based on preoperative lab testing and could not have other significant comorbidities that precluded surgical intervention.

*Intraoperative procedure*. Pancreatic resection was performed using standard techniques, and major surgical complications were defined as previously described (39). Gemcitabine was administered intravenously at 500 mg/m$^2$ for the first 2 patients (per IRB safety recommendations), then subsequently at 1,000 mg/m$^2$ with an infusion pump at a fixed dose rate of 10 mg/m$^2$/min (over 50 and 100 minutes, respectively) and was delivered at the start of operation and concluded prior to specimen removal. Serum samples were collected at regular intervals during the operation to determine gemcitabine pharmacokinetics (Figure 2C).

*Toxicity monitoring*. The M.D. Anderson Data and Safety Monitoring Board oversaw the study. Drug toxicities were evaluated according to Common Terminology Criteria for Adverse Events version 3.0. Daily postoperative labs, including absolute neutrophil counts (ANC) and platelet counts, were obtained. Patients received full supportive care, and the use of growth factors was permitted for myelosuppression (ANC < $0.5 \times 10^9$). There were 3 patients with grade III neutropenia or leukopenia, and 3 patients with grade II neutropenia. All cytopenias were transient with nadir at approximately postoperative day 6 (Supplemental Figure 5). No significant thrombocytopenia occurred in any patients. There were 2 patients given GM-CSF empirically, and there were no infectious complications in the whole cohort.

*Pathological analysis*. Immediately after specimen collection, tumors were bivalved by a surgical pathologist, and 4.0-mm punch biopsies were taken from the outer and inner portions of the tumors (median 4 samples per tumor) as well from as the normal pancreas. The punch biopsies were sent for quantitative analysis of the gemcitabine metabo-

lite incorporation into the DNA of the cells within the pancreatic tumor (i.e., cancer and stromal cells) and normal pancreas (Advion BioServices; Supplemental Figures 2 and 3 and ref. 40). The tumor and normal pancreatic tissue surrounding each punch biopsy site were submitted for histologic confirmation of the tissue type (tumor vs. normal) and assessment of stromal score by H&E and Masson trichrome stains, hENT1 (percentage of cells with staining intensity relative to lymphocyte control, scored as 0 [no staining], 1+ [low staining], 2+ [equivalent staining], or 3+ [high staining]; MBL International) (17), and Ki67 (percentage of cells with staining; MBL International).

### *Statistics*

JMP 10.0 (SAS Institute) was used to perform all statistical analyses. All data were tested for normal distribution using the D'Agostino and Pearson omnibus normality test, where a *P* value greater than 0.05 was considered to pass the normality test. Supplemental Table 11 summarizes normality tests for the data. Mann-Whitney (Wilcoxon) test was used to compare distributions between groups, and Spearman rank-order test was used for nonparametric correlation analysis, as appropriate. Linear regression (ANOVA) was used for correlations as long as normal distribution assumptions were met. All linear regression analyses are shown with the linear curve fit and 95% CI shaded in blue. Survival curves were constructed using the Kaplan-Meier method. The Cox proportional-hazards model was used for univariate and multivariate survival analyses. Variables were included in the multivariate Cox proportional-hazards model if the *P* value was 0.15 or less, or if variables were previously demonstrated to influence outcome. A *P* value less than 0.05 was considered significant for all analyses.

### *Study approval*

All patients in the study were part of IRB-approved protocols. The prospective trial of intraoperative gemcitabine (Clinicaltrials.gov NCT01276613) only included patients who signed written informed consent for the study. Retrospective analyses were approved by the IRB for waiver of informed consent.

## Acknowledgments

This research was primarily supported by research funds provided by the Lustgarten Foundation (989161) and by The Methodist Hospital Research Institute, including the Ernest Cockrell Jr. Distinguished Endowed Chair and NIH's Physical Sciences Oncology Centers (PSOCs) U54CA143837, Center for Transport Oncophysics. The authors also acknowledge partial support from the Department of Defense (W81XWH-09-1-0212), NIH (U54CA151668 and U54CA149196), and NSF (DMS-1263742). E.J. Koay received support from the Anne Eastland Spears Fellowship for GI Cancer Research. M.J. Truty received support from NCI/NIH Paul Calabresi Clinical Investigator K12 (KCA088084). V. Cristini was supported by the Ruby Hansen Surface Professorship in Molecular Modeling of Cancer. The authors also acknowledge the scientific editing support of Christine Wogan.

Received for publication October 2, 2013, and accepted in revised form January 3, 2014.

Address correspondence to: Jason B. Fleming, T. Boone Pickens Academic Tower, 1515 Holcombe Blvd., Unit 1484, Houston, Texas 77030, USA. Phone: 713.745.0890; Fax: 713.745.4426; E-mail: jbflemin@mdanderson.org.

1. Lockhart AC, Rothenberg ML, Berlin JD. Treatment for pancreatic cancer: current therapy and continued progress. *Gastroenterology*. 2005;128(6):1642–1654.
2. Li D, Xie K, Wolff R, Abbruzzese JL. Pancreatic cancer. *Lancet*. 2004;363(9414):1049–1057.
3. Olive KP, et al. Inhibition of Hedgehog signaling enhances delivery of chemotherapy in a mouse model of pancreatic cancer. *Science*. 2009; 324(5933):1457–1461.
4. Beatty GL, et al. CD40 agonists alter tumor stroma and show efficacy against pancreatic carcinoma in mice and humans. *Science*. 2011; 331(6024):1612–1616.
5. Frieboes HB, Chaplain MA, Thompson AM, Bearer EL, Lowengrub JS, Cristini V. Physical oncology: a bench-to-bedside quantitative and predictive approach. *Cancer Res*. 2011;71(2):298–302.
6. Jain RK. Transport of molecules across tumor vasculature. *Cancer Metastasis Rev*. 1987;6(4):559–593.
7. Michor F, Liphardt J, Ferrari M, Widom J. What does physics have to do with cancer? *Nat Rev Cancer*. 2011;11(9):657–670.
8. Ferrari M. Frontiers in cancer nanomedicine: directing mass transport through biological barriers. *Trends Biotechnol*. 2010;28(4):181–188.
9. Neesse A, et al. Stromal biology and therapy in pancreatic cancer. *Gut*. 2011;60(6):861–868.
10. Edgerton ME, Chuang YL, Macklin P, Yang W, Bearer EL, Cristini V. A novel, patient-specific mathematical pathology approach for assessment of surgical volume: application to ductal carcinoma in situ of the breast. *Anal Cell Pathol (Amst)*. 2011;34(5):247–263.
11. Pascal J, Bearer EL, Wang Z, Koay EJ, Curley SA, Cristini V. Mechanistic patient-specific predictive correlation of tumor drug response with microenvironment and perfusion measurements. *Proc Natl Acad Sci U S A*. 2013;110(35):14266–14271.
12. Pries AR, Hopfner M, le Noble F, Dewhirst MW, Secomb TW. The shunt problem: control of functional shunting in normal and tumour vasculature. *Nat Rev Cancer*. 2010;10(8):587–593.
13. Provenzano PP, Cuevas C, Chang AE, Goel VK, Von Hoff DD, Hingorani SR. Enzymatic targeting of the stroma ablates physical barriers to treatment of pancreatic ductal adenocarcinoma. *Cancer Cell*. 2012;21(3):418–429.
14. Stylianopoulos T, et al. Causes, consequences, and remedies for growth-induced solid stress in murine and human tumors. *Proc Natl Acad Sci U S A*. 2012;109(38):15101–15108.
15. Farrell JJ, et al. Human equilibrative nucleoside transporter 1 levels predict response to gemcitabine in patients with pancreatic cancer. *Gastroenterology*. 2009;136(1):187–195.
16. McNulty NJ, Francis IR, Platt JF, Cohan RH, Korobkin M, Gebremariam A. Multi-detector row helical CT of the pancreas: effect of contrast-enhanced multiphasic imaging on enhancement of the pancreas, peripancreatic vasculature, and pancreatic adenocarcinoma. *Radiology*. 2001;220(1):97–102.
17. Morinaga S, et al. Immunohistochemical analysis of human equilibrative nucleoside transporter-1 (hENT1) predicts survival in resected pancreatic cancer patients treated with adjuvant gemcitabine monotherapy. *Ann Surg Oncol*. 2012;19(suppl 3):S558–S564.
18. Zhao Q, et al. Pathologic complete response to neoadjuvant therapy in patients with pancreatic ductal adenocarcinoma is associated with a better prognosis. *Ann Diagn Pathol*. 2012;16(1):29–37.
19. Evans DB, et al. Preoperative gemcitabine-based chemoradiation for patients with resectable adenocarcinoma of the pancreatic head. *J Clin Oncol*. 2008;26(21):3496–3502.
20. Varadhachary GR, et al. Preoperative gemcitabine and cisplatin followed by gemcitabine-based chemoradiation for resectable adenocarcinoma of the pancreatic head. *J Clin Oncol*. 2008;26(21):3487–3495.
21. Chatterjee D, et al. Histologic grading of the extent of residual carcinoma following neoadjuvant chemoradiation in pancreatic ductal adenocarcinoma: a predictor for patient outcome. *Cancer*. 2012;118(12):3182–3190.
22. National Cancer Institute. Cancer Trends Progress Report 2011/2012. NIH Web site. http://progressreport.cancer.gov/. Accessed January 31, 2014.
23. Nagaraju GP, El-Rayes BF. SPARC and DNA methylation: possible diagnostic and therapeutic implications in gastrointestinal cancers. *Cancer Lett*. 2013;328(1):10–17.
24. Penchev VR, Rasheed ZA, Maitra A, Matsui W. Heterogeneity and targeting of pancreatic cancer stem cells. *Clin Cancer Res*. 2012;18(16):4277–4284.
25. Kindler HL, et al. Axitinib plus gemcitabine versus placebo plus gemcitabine in patients with advanced pancreatic adenocarcinoma: a double-blind randomised phase 3 study. *Lancet Oncol*. 2011; 12(3):256–262.
26. Schmidt J, et al. Open-label, multicenter, randomized phase III trial of adjuvant chemoradiation plus interferon Alfa-2b versus fluorouracil and folinic acid for patients with resected pancreatic adenocarcinoma. *J Clin Oncol*. 2012;30(33):4077–4083.
27. Crane CH, Iacobuzio-Donahue CA. Keys to personalized care in pancreatic oncology. *J Clin Oncol*. 2012;30(33):4049–4050.
28. Pascal J, et al. Mechanistic modeling identifies drug-uptake history as predictor of tumor drug resistance and nano-carrier-mediated response. *ACS Nano*. 2013;7(12):11174–11182.
29. Tofts PS, et al. Estimating kinetic parameters from dynamic contrast-enhanced T(1)-weighted MRI of a diffusable tracer: standardized quantities and symbols. *J Magn Reson Imaging*. 1999;10(3):223–232.
30. Wasser K, et al. Evaluation of neoadjuvant chemotherapeutic response of breast cancer using dynamic MRI with high temporal resolution. *Eur Radiol*. 2003;13(1):80–87.
31. Park MS, et al. Perfusion CT: noninvasive surrogate marker for stratification of pancreatic cancer response to concurrent chemo- and radiation therapy. *Radiology*. 2009;250(1):110–117.
32. Kawada N, et al. Human equilibrative nucleoside transporter 1 level does not predict prognosis in

pancreatic cancer patients treated with neoadjuvant chemoradiation including gemcitabine. *J Hepatobiliary Pancreat Sci*. 2012;19(6):717–722.
33. Eisbruch A, et al. Radiation concurrent with gemcitabine for locally advanced head and neck cancer: a phase I trial and intracellular drug incorporation study. *J Clin Oncol*. 2001;19(3):792–799.
34. Taghian AG, et al. Paclitaxel decreases the interstitial fluid pressure and improves oxygenation in breast cancers in patients treated with neoadjuvant chemotherapy: clinical implications. *J Clin Oncol*. 2005;23(9):1951–1961.
35. Papadopoulos N, Kinzler KW, Vogelstein B. The role of companion diagnostics in the development and use of mutation-targeted cancer therapies. *Nat Biotechnol*. 2006;24(8):985–995.
36. Tamm EP, Balachandran A, Bhosale P, Szklaruk J. Update on 3D and multiplanar MDCT in the assessment of biliary and pancreatic pathology. *Abdom Imaging*. 2009;34(1):64–74.
37. Bae KT. Intravenous contrast medium administration and scan timing at CT: considerations and approaches. *Radiology*. 2010;256(1):32–61.
38. Varadhachary GR, et al. Borderline resectable pancreatic cancer: definitions, management, and role of preoperative therapy. *Ann Surg Oncol*. 2006; 13(8):1035–1046.
39. Evans D, Lee J, Tamm E. Pancreaticoduodenectomy (Whipple Operation) and total pancreatectomy for cancer. In: Fischer JF, ed. *Fischer's Mastery of Surgery*. 5th ed. Philadelphia, Pennsylvania, USA: Lippincott Williams and Wilkins; 2007:Chapter 113.
40. Wickremsinhe ER, et al. Quantification of gemcitabine incorporation into human DNA by LC/MS/MS as a surrogate measure for target engagement. *Anal Chem*. 2010;82(15):6576–6583.